A Single-Shot and Real-Time 3D Imaging Technique for Facial Motion Capture Based on Triple-Frequency Color Fringe Projection

Xiang ZHOU *[a,b], Zhuangqun YANG[c], Tao YANG[a], Hong ZHAO[a]
[a]State Key Laboratory Manufacturing Systems Engineering, Xi'an Jiaotong University, Xi'an, Shaanxi, China;
[b]School of Physical Sciences, University of Kent, Canterbury, UK;
[c]The First Affiliated Hospital of Medical College of Xi'an Jiaotong University, Xi'an, Shaanxi, China

Abstract

Fast and high-accuracy 3D imaging is playing an important role in scanning human face sunder dynamical change. This paper presents a single-shot technique for real-time surface profiling and texture retrieving of human face. In this technique, three fringe patterns with a carrier frequency ratio of 1:3:9 are encoded in the red (R), green (G) and blue (B) channels of a color fringe pattern and projected onto the object's surface by a 3-LCD projector. The deformed color fringe pattern is captured by color CCD from another angle. The cross talk among color channels of commercial CCD and projector is modeled as the color coupling equations. Then FFT-Spectrum minimization and bi-dimensional empirical mode decomposition (BEMD) are employed to solve the equations, thereby extracting the low, medium and high fundamental frequency components from R, G and B patterns. 2D-FFT is performed to retrieve wrapping phase distributions of three components. Afterwards, a three-step phase unwrapping strategy is formulated to recursively unwrap phases from low, medium and high carrier patterns. Unwrapped phase of the high-frequency component is selected to recover the object's height distribution. Apart from the shape, textures of objects are as well retrieved by solving the color coupling equations, facilitating 3D real construction combined with textures. The algorithm is accelerated by GPU parallel computation, fulfilling so far 1 frame/s 3D real reconstruction.

Keywords: 3d body scanning, facial motion capture, fringe pattern projection, texture extraction

1. Introduction

With the rapid development in computer technology, 3D shape measurement, especially for dynamic objects in fast motion, has found wide applications, such as 3D movies and games, web 3D, online quality inspection, human computer interaction, facial expression capture, plastic surgery and so on. For real-time 3D shape measurement, the sampled data have to be acquired rapidly, processed quickly, and displayed in a very short period of time. Over the past years, various optical techniques have been developed for real-time 3D shape measurement [1]. Time-of-flight (TOF) is one of the techniques that has been commercially used [2]. However, accuracy is affected by its fundamental limitations. Stereo vision is another technique widely studied and extensively used [2]. Although this technique could maximize the camera's data acquisition speed, matching the stereo images is time-consuming and very difficult for uncharacteristic objects.

Fringe projection is a relatively simple technique with merits of well-established and fast processing speed. It has found large-scale applications in measuring the 3D shape of dynamic objects. Shape measurement using this technique is carried out by extracting the phase distribution of the fringes. The phase shifting approach has high accuracy and large measurement range, but the phase stepping process is time-consuming. By contrast, the Fourier transform approach requires only one fringe pattern, but its measurement range and accuracy is limited by spectrum aliasing [3].

Dynamic measurement may be implemented in a very short time via two ways. One way is to use a single pattern which can be a composite gray [4-6] or color fringe pattern [7-13]. For the gray pattern-based methods, multi-frequency fringes or crossed fringes are composed in a single pattern and projected onto the object's surface. Fourier transform is often used to separate the components of composite fringes and retrieve the wrapped phase, which is unwrapped by different phase unwrapping algorithms. However, its measurement range and accuracy are limited by spectrum aliasing. By comparison, color pattern-based techniques could provide more information, but the measurement results are always affected by the variations of the object's surface color and the cross talk among the color channels of commercial CCD and projector. One solution to color decoupling is to add light filters and use a three-chip CCD [7], which inevitably decreases light sensitivity and increases hardware cost.

*Corresponding author: zhouxiang@mail.xjtu.edu.cn

The other solution is calibrating the coefficients with coupling effects among color channels, which would lead to different results depending on the choice of projector, CCD, and the variation of the object's surface color [7-9, 11].
The other way for boosting measuring the speed is to use multiple patterns, while switching them rapidly so that the patterns required for reconstructing 3D shape can be captured in a short period of time. Huang and Zhang et al. proposed a new phase-shifting method using color patterns. Based on the digital projector, the shape acquisition speed can reach 30 fps [14, 15]. However, dynamic objects with very high speed may be difficult to measure. In addition, information for phase unwrapping, particularly in measuring large geometries, is insufficient.
This paper presents a single-shot technique for real-time surface profiling and texture retrieving of human faces. In this technique, three fringe patterns with a carrier frequency ratio of 1:3:9 are encoded in the red (R), green (G) and blue (B) channels of a color fringe pattern and projected onto the object's surface by a 3-LCD projector. The deformed color fringe pattern is captured by color CCD from another angle. The cross talk among color channels of commercial CCD and projector is modeled as the color coupling equations. Then FFT-Spectrum minimization and bi-dimensional empirical mode decomposition (BEMD) are employed to solve the equations, thereby extracting the low, medium and high fundamental frequency components from R, G and B patterns. 2D-FFT is performed to retrieve wrapping phase distributions of three components. Afterwards, a three-step phase unwrapping strategy is formulated to recursively unwrap phases from low, medium and high carrier patterns. Unwrapped phase of the high-frequency component is selected to recover the object's height distribution. Apart from the shape, textures of objects are as well retrieved by solving the color coupling equations, facilitating 3D real construction combined with textures.
The proposed technique is featured as high accuracy, single shot and real-time computation. The phase unwrapping problem, which is conventionally solved by sequentially projecting varying period fringes in temporal domain, is now tackled by projecting color fringe pattern and solving the color coupling equations, making possible a short period of fringes. So the accuracy of the retrieved shape can be as high as fringe-projected techniques of static objects. Benefiting from a single shot, the proposed technique is able to measure moving and varying objects with large discontinuity or spatially isolated surfaces. The BEMD above, which accounts for the major part of total computation, is implemented with a morphological imaging processing algorithm and accelerated by GPU parallel computation, fulfilling so far 1 frame/s 3D real reconstruction. Given an improvement of hardware, frame speed would potentially increase to 10 frame/s.

2. Principles

2.1. Color fringe-projection and color coupling equations

The classic crossed-optical-axes geometry model for color fringe-projected technique is shown in Fig. 1. The optical axis of the projector lens *PO* crosses that of the camera lens *CO* at point *O* on the reference plane and the angle between them is *θ*. *H* is a point on the object's surface, whereas *A* and *B* denote two points on the reference plane. $h(x, y)$ is the height distribution of the object. *L* and *d* denote the distance between *C* and *O* and *C* and *P*, respectively.

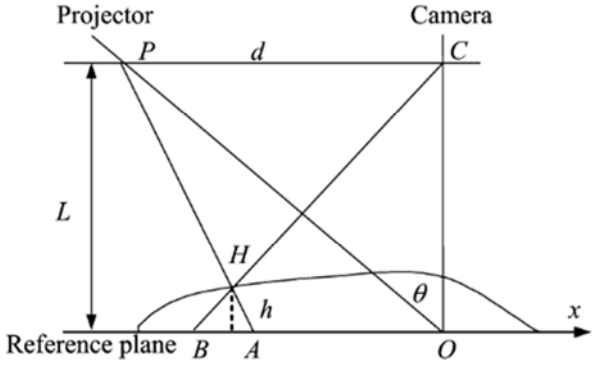

Fig. 1 Optical geometry.

Three sinusoidal fringe patterns with 1:3:9 carrier frequency ratio, expressed as Eq. (1), are encoded into the red, green and blue channels of a color image, respectively, and then projected on the tested object by an LCD projector.

$$\begin{bmatrix} R(x,y) \\ G(x,y) \\ B(x,y) \end{bmatrix} = \begin{bmatrix} a_r \\ a_g \\ a_b \end{bmatrix} + \begin{bmatrix} b_r \cos(2\pi f_r x) \\ b_g \cos(2\pi f_g x) \\ b_b \cos(2\pi f_b x) \end{bmatrix}, \quad (1)$$

where $\{a_i, i = r,g,b\}$ represent the background intensities of the red, green and blue fringe patterns, $\{b_i, i = r,g,b\}$ represent their amplitudes, and $f_r : f_g : f_b = 1:3:9$ are the carrier frequencies. A CCD is used to capture the deformed color fringe pattern from another angle. The deformed color fringe patterns with the coupling effect among color channels can be expressed as

$$\begin{bmatrix} g_r(x,y) \\ g_g(x,y) \\ g_b(x,y) \end{bmatrix} = \begin{bmatrix} C_{rr} & C_{rg} & C_{rb} \\ C_{gr} & C_{gg} & C_{gb} \\ C_{br} & C_{bg} & C_{bb} \end{bmatrix} \begin{bmatrix} r_r(x,y) \cdot \{a_r + b_r \cos[2\pi f_r x + \Phi_r(x,y)]\} \\ r_g(x,y) \cdot \{a_g + b_g \cos[2\pi f_g x + \Phi_g(x,y)]\} \\ r_b(x,y) \cdot \{a_b + b_b \cos[2\pi f_b x + \Phi_b(x,y)]\} \end{bmatrix}, \quad (2)$$

where $\{C_{ij} \le 1, i,j = r,g,b\}$ are the coefficients representing the coupling effects among color channels and $C_{ij} = 1$ if $i = j$. $\{r_i(x,y), i = r,g,b\}$ are the reflectivity distributions. $\{n_i(x,y), i = r,g,b\}$ indicate the noise. $\{\Phi_i(x,y), i = r,g,b\}$ represent the phase modulation caused by height distribution $h(x,y)$. We denote $A_i(x,y) = r_i(x,y)a_i$, $B_i(x,y) = r_i(x,y)b_i$, $(i = r,g,b)$, and Eq. (2) then is replaced with

$$\begin{bmatrix} g_r(x,y) \\ g_g(x,y) \\ g_b(x,y) \end{bmatrix} = \begin{bmatrix} C_{rr} & C_{rg} & C_{rb} \\ C_{gr} & C_{gg} & C_{gb} \\ C_{br} & C_{bg} & C_{bb} \end{bmatrix} \begin{bmatrix} A_r(x,y) + B_r(x,y)\cos[2\pi f_r x + \Phi_r(x,y)] \\ A_g(x,y) + B_g(x,y)\cos[2\pi f_g x + \Phi_g(x,y)] \\ A_b(x,y) + B_b(x,y)\cos[2\pi f_b x + \Phi_b(x,y)] \end{bmatrix}. \quad (3)$$

when $L >> h(x,y)$,

$$h(x,y) = -\frac{L\Delta\Phi_i(x,y)}{2\pi f_i d} = -\frac{L}{2\pi f_i d}\left[\Phi_i(x,y) - \Phi_{0i}(x,y)\right], (i = r,g,b), \quad (4)$$

Where $\{\Phi_{0i}(x,y), i = r,g,b\}$ are the phase value of the fringe pattern on reference plane. Eq. (3) is named as the color coupling equations(CCE).

Our ultimate goal is to obtain the unwrapped phase $\Delta\Phi_b(x,y)$ ($\Delta\Phi_b(x,y) = \Phi_b(x,y) - \Phi_{0b}(x,y)$) of the high-frequency fringe, from which the height distribution of the object is recovered. To achieve this goal, two problems which are phase extraction and phase unwrapping have to be solved.

Conventionally, phase extraction can be fulfilled by Fourier transform[3] which filters out all but fundamental frequency components in frequency domain and extracts phase after inverse FFT. However, in this method the cross talks among channels impede the complete extraction of the fundamental frequency components. To decouple the cross talks, a BEMD-based algorithm is presented in section 2.2.

Once the phase maps of high-, medium- and low-frequency fringe patterns are obtained phase unwrapping can be easily implemented by a three-step phase unwrapping strategy which is described in section 2.3.

2.2. Solution to the color coupling equations

2.2.1. The simplification of the color coupling equations

For convenience, Eq. (3) is rewritten as

$$\begin{bmatrix} g_r(x,y) \\ g_g(x,y) \\ g_b(x,y) \end{bmatrix} = \begin{bmatrix} C_{rr} & C_{rg} & C_{rb} \\ C_{gr} & C_{gg} & C_{gb} \\ C_{br} & C_{bg} & C_{bb} \end{bmatrix} \begin{bmatrix} A_r(x,y) \\ A_g(x,y) \\ A_b(x,y) \end{bmatrix} + \begin{bmatrix} C_{rr} & C_{rg} & C_{rb} \\ C_{gr} & C_{gg} & C_{gb} \\ C_{br} & C_{bg} & C_{bb} \end{bmatrix} \begin{bmatrix} B_r(x,y)COS_r(x,y) \\ B_g(x,y)COS_g(x,y) \\ B_b(x,y)COS_b(x,y) \end{bmatrix}, \quad (5)$$

where $\{COS_i(x,y) = \cos[2\pi f_i x + \Phi_i(x,y)],\ i = r,g,b\}$. If the object surface is assumed to be monochromatic the following replacement holds.

$$\begin{bmatrix} A_r(x,y) \\ A_g(x,y) \\ A_b(x,y) \end{bmatrix} = \begin{bmatrix} r_a A(x,y) \\ r_b A(x,y) \\ r_c A(x,y) \end{bmatrix}, \quad (6)$$

where $\{r_i, i = r,g,b\}$ represent ratios of reflectivity unbalance among channels. Thus Eq. (5) can be further simplified as

$$\begin{bmatrix} g_r(x,y) \\ g_g(x,y) \\ g_b(x,y) \end{bmatrix} = A(x,y) \begin{bmatrix} C_{rr}r_a + C_{rg}r_b + C_{rb}r_c \\ C_{gr}r_a + C_{gg}r_b + C_{gb}r_c \\ C_{br}r_a + C_{bg}r_b + C_{bb}r_c \end{bmatrix} + \begin{bmatrix} C_{rr} & C_{rg} & C_{rb} \\ C_{gr} & C_{gg} & C_{gb} \\ C_{br} & C_{bg} & C_{bb} \end{bmatrix} \begin{bmatrix} B_r(x,y)COS_r(x,y) \\ B_g(x,y)COS_g(x,y) \\ B_b(x,y)COS_b(x,y) \end{bmatrix}. \quad (7)$$

The Eq. (7) can be further simplified as

$$\begin{bmatrix} g_r(x,y) \\ g_g(x,y) \\ g_b(x,y) \end{bmatrix} = \begin{bmatrix} C_{rr} & C_{rg} & C_{rb} & N_r \\ C_{gr} & C_{gg} & C_{gb} & N_g \\ C_{br} & C_{bg} & C_{bb} & N_b \end{bmatrix} \begin{bmatrix} B_r(x,y)COS_r(x,y) \\ B_g(x,y)COS_g(x,y) \\ B_b(x,y)COS_b(x,y) \\ A(x,y) \end{bmatrix} \quad (8)$$

where

$$\begin{bmatrix} N_r \\ N_g \\ N_b \end{bmatrix} = \begin{bmatrix} C_{rr}r_a + C_{rg}r_b + C_{rb}r_c \\ C_{gr}r_a + C_{gg}r_b + C_{gb}r_c \\ C_{br}r_a + C_{bg}r_b + C_{bb}r_c \end{bmatrix}. \quad (9)$$

This 3x4 matrix is named as “the coupling coefficient matrix (CCM)” in the following text. In order to extract the fundamental frequency components, i.e., $\{B_i(x,y)COS_i(x,y),\ i=r,g,b\}$ FFT-Spectrum minimization and BEMD are subsequently employed to calibrate CCM and solve the Eq. (8).

2.2.2. Calibration of the coupling coefficient matrix

As shown in Eq. (8) the elements of R, G, B channels from the any given component out of $\{B_i(x,y)COS_i(x,y),\ i=r,g,b\}$ and $A(x,y)$ differ in only a factor. On top of that, the elements from different components are located in different bands in frequency domain. Therefore, a scheme based on FFT-Spectrum minimization is used to calibrate the CCM. Specifically, it can be achieved by solving the following optimization problems:

$$\min_{d_i}\left\{\sum_{u,v} w_{DC}(u,v)\left|\hat{g}_r(u,v) - d_i\cdot\hat{g}_i(u,v)\right|\right\},\quad i=g,b \quad (10)$$

$$\min_{h_i}\left\{\sum_{u,v} w_{H}(u,v)\left|\hat{g}_r(u,v) - h_i\cdot\hat{g}_i(u,v)\right|\right\},\quad i=g,b \quad (11)$$

$$\min_{m_i}\left\{\sum_{u,v} w_{M}(u,v)\left|\hat{g}_r(u,v) - m_i\cdot\hat{g}_i(u,v)\right|\right\},\quad i=g,b \quad (12)$$

$$\min_{l_i}\left\{\sum_{u,v} w_{L}(u,v)\left|\hat{g}_r(u,v) - l_i\cdot\hat{g}_i(u,v)\right|\right\},\quad i=g,b \quad (13)$$

where $\hat{g}_r(u,v)$ and $\hat{g}_i(u,v)$ are 2D FT of $g_r(x,y)$ and $g_i(x,y)$, respectively. We will use the hat symbol to represent the 2D FT throughout this paper. $w_{DC}(u,v)$ is a window function centered at zero frequency. In the same way, $w_{DC}(u,v)$, $w_{DC}(u,v)$ and $w_{DC}(u,v)$ are centered at high, medium, low carrier frequencies, respectively. In fact, Eq. (10) is an unconstrained linear minimization to find d_i that is a local minimum to a scalar function, so are Eqs. (11)-(13). As a result, we can obtain the following relationship among coefficients:

$$\begin{bmatrix} C_{rr} \\ C_{rg} \\ C_{rb} \\ N_r \end{bmatrix} = \begin{bmatrix} l_i C_{ir} \\ m_i C_{ig} \\ h_i C_{ib} \\ d_i N_i \end{bmatrix},\quad i=g,b. \quad (14)$$

Hence, the number of unknown coefficients is reduced to four through the calibration. Furthermore, if $\left[C_{rr}B_r(x,y)COS_r(x,y)\quad C_{rg}B_g(x,y)COS_g(x,y)\quad C_{rb}B_b(x,y)COS_b(x,y)\quad N_rA(x,y)\right]$ in Eq. (8) are viewed as four unknown variables only one additional condition is needed to produce a unique solution. Therefore, an additional method is necessary to help solve the equation, which is described in the following section.

2.2.3. Extraction of the fundamental frequency components

Given $g_r(x,y)$ and $g_g(x,y)$, the removal of $A(x,y)$ can be achieved by solving the following optimization problem:

$$\min_k \left\{ \sum_{u,v} w_{DC}(u,v) \left| \hat{g}_g(u,v) - k \cdot \hat{g}_r(u,v) \right| \right\}, \tag{15}$$

As a result, we can obtain the difference $g_{b-r}(x,y) = g_b(x,y) - k \cdot g_r(x,y)$ in which the background $A(x,y)$ is eliminated. That is

$$g_{b-r}(x,y) = \begin{bmatrix} C_{br} - kC_{rr} \\ C_{bg} - kC_{rg} \\ C_{bb} - kC_{rb} \end{bmatrix}^T \begin{bmatrix} B_r(x,y)COS_r(x,y) \\ B_g(x,y)COS_g(x,y) \\ B_b(x,y)COS_b(x,y) \end{bmatrix}. \tag{16}$$

As shown in Eq. (16), $g_{b-r}(x,y)$ is a combination of three carrier components from high to low frequency except the background intensity $A(x,y)$. Next, a so-called Morphological operation-based BEMD (MOBEMD) is applied to extract the fundamental frequency component of the high carrier from $g_{b-r}(x,y)$ because MOBEMD has a good performance on separating this kind of mixed patterns[16]. The instinct mode function (IMF) resulted from MOBEMD of $g_{b-r}(x,y)$ is approximately equal to the 3rd term in Eq. (16), denoted as $F_b(x,y) = (C_{bb} - k_1 C_{rb}) B_b(x,y)COS_b(x,y)$. That is, the fundamental frequency component of the high carrier pattern is completely separated.

Next, $F_b(x,y)$ is used to estimate the high frequency elements in Eq. (8) through the following minimization.

$$\min_e \left\{ \sum_{u,v} \left| \hat{g}_r(u,v) - e \cdot \hat{F}_b(u,v) \right| \right\}, \tag{17}$$

So

$$C_{rb} B_b(x,y)COS_b(x,y) = e \cdot F_b(x,y). \tag{18}$$

As a result, the number of unknown variables in Eq. (8) is reduced to three which means there exists a unique solution to the equations. That is, all the elements in Eq. (8) can be resolved.

2.3. Three-step phase unwrapping

Given the selected elements $\left[C_{rr}B_r(x,y)COS_r(x,y) \quad C_{gg}B_g(x,y)COS_g(x,y) \quad C_{bb}B_b(x,y)COS_b(x,y) \right]$ in Eq. (8), phase distribution $\{\Phi_i(x,y), i = r,g,b\}$ of the three fringe patterns can be easily demodulated via 2D Fourier transform without any spectrum aliasing.

Similarly, the phase value of the fringe pattern on reference plane $\{\Phi_{0i}(x,y), i = r,g,b\}$ can be extracted by the same strategy.

The phase ($\Delta\varphi_i(x,y), (i = r,g,b)$) demodulated via 2D Fourier transform is wrapped from $-\pi$ to π and must be unwrapped. A three-step phase unwrapping strategy is developed, according to the temporal phase unwrapping strategy proposed by H. Zhao et al. [17]. The phase distribution of low-frequency fringe with the least wraps or even no wrap is used to unwrap that of the medium, then the medium unwraps the high. Finally, the unwrapped phase distribution of high-frequency fringe is retrieved to recover the height distribution of the object. The wrapped phase is unwrapped point by point, from one phase map to another, without the help of the neighboring points' phase. Therefore, the process is very fast and reliable. Suppose the unwrapped phase values are denoted as $\Delta\Phi_i(x,y), (i = r,g,b)$, and given by

$$\Delta\Phi_r(x,y) = \Delta\varphi_r(x,y), \tag{19}$$

$$\Delta\Phi_i(x,y) = \Delta\varphi_i(x,y) + 2n_i(x,y)\pi, (i = g,b). \tag{20}$$

The three-step phase unwrapping strategy is described in detail as follows:

Step 1.The phase distribution of the low-frequency fringe with the least wraps or even no wrap is used to unwrap that of the medium-frequency fringe.

$$n_G(x,y) = INT\left[\frac{\Delta\Phi_g(x,y)}{2\pi}\right] = INT\left[\frac{k_r\Delta\Phi_r(x,y)/k_g - \Delta\varphi_g(x,y)}{2\pi}\right], \quad (21)$$

where INT is an operator equal to the integer part of its argument, and k_r, k_g are isolated constants determined by Eq. (4): $k_r = -\frac{L}{2\pi f_r d}$, $k_g = -\frac{L}{2\pi f_g d}$.

Step 2.Considering the influence of noise and calibration errors, the result obtained by Eq. (21) should be revised. Define the difference between the height distributions obtained from the medium and low-frequency fringes as the quantity:

$$\Delta(m) = k_g\left[\Delta\varphi_g(x,y) + 2m\pi\right] - k_r\Delta\Phi_r(x,y), \left[m = n_G(x,y), n_G(x,y)\pm 1\right], \quad (22)$$

m is termed $m_{0g}(x,y)$ when $\Delta(m)$ reaches its minimum. Finally, the unwrapped distribution $\Delta\Phi_g(x,y)$ is:

$$\Delta\Phi_g(x,y) = \Delta\varphi_g(x,y) + 2m_{0g}(x,y)\pi. \quad (23)$$

Step 3.Subsequently, the unwrapped phase distribution of the medium-frequency fringe $\Delta\Phi_g(x,y)$ is used to unwrap $\Delta\varphi_b(x,y)$, resulting in $\Delta\Phi_b(x,y)$.

3. Computer simulations

Based on Eq. (2), a 512 × 512 pixel image of a deformed color fringe pattern contaminated by Gaussian white noise with constant mean and variance was generated by the computer software and shown in Fig. 2. The color coupling effects of commercial CCDs and projectors vary from one combination to another, but the coefficients are normally between 0.1-0.4 according to our experience and Ref. [18]. For simplicity, the uniform coefficient value is simulated, ignoring the minor difference among channels. Specifically, the coupling coefficients C_{ij} were set to 0.2 if $i \neq j$, and 1 if $i = j$; that is, $\{C_{ij} = 0.2, i \neq j; C_{ij} = 1, i = j\}$. The background intensities and their amplitudes were set to 40 and 18 respectively. Other parameters were set as follows:

- Normalized carrier frequencies: $f_r = 1/128, f_g = 3f_r, f_b = 9f_r$.
- Phase distribution: $\Phi_r(x,y) = P(x,y), \Phi_g(x,y) = 3P(x,y), \Phi_b(x,y) = 9P(x,y)$; where,

$$P(x,y) = 3[3(1-x)^2 e^{-x^2-(y+1)^2} - 10(\frac{x}{5} - x^3 - y^5)e^{-x^2-y^2} - \frac{1}{3}e^{-(x+1)^2-y^2}]/8, (x,y = 1,2\cdots 512).$$

And it can be generated by the peaks function provided by the MATLAB function base.

- The reflectivity distribution: $\{r_i(x,y) = 3 + 40\Phi_r'(x,y), i = r,g,b\}$.

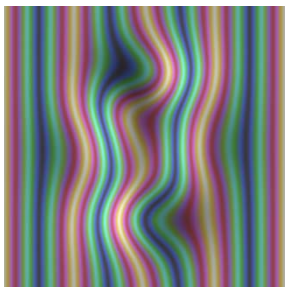

Fig. 2 Deformed color fringe pattern.

The true fundamental frequency components of the deformed color fringe pattern are shown in Fig. 3(a)–3(c), whereas those extracted by color decoupling algorithm based on BEMD are shown in Fig. 3(d)–3(f). The low, medium and high fundamental frequency components are extracted accurately without mode mixing. Then the wrapped phase distribution of the three fringe patterns (as shown in Fig. 4(a)–4(c)) is demodulated via 2D Fourier transform, followed by phase unwrapping using three-step phase unwrapping strategy. Fig. 4(d) and 4(e) show the unwrapped phase maps of the medium and high-frequency fringes, respectively, and 4(f) is the absolute error map. The maximum of the absolute error map is 0.3408, only 0.69% of the peak value. This result shows that the method can achieve high precision.

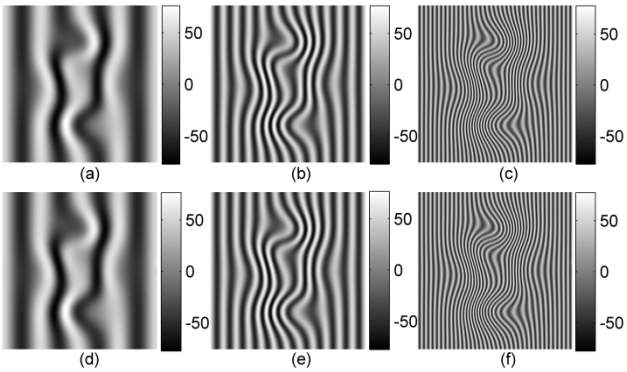

Fig. 3 True (a) low, (b) medium, and (c) high fundamental frequency components, and (d) low, (e) medium and (f) high ones extracted by color decoupling algorithm based on BEMD.

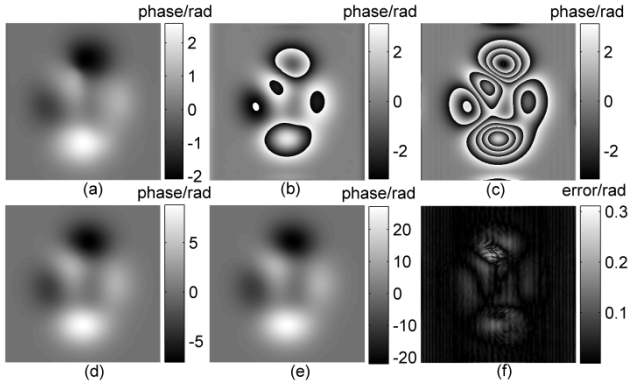

Fig. 4 Wrapped phase distribution of (a) low, (b) medium and (c) high-frequency fringes, and unwrapped phase maps of (d) medium and (e) high-frequency fringes, and (f) absolute error map.

4. Experiments

The experimental setup in Fig. 5 (a) was applied in our experiments. We used Sony VPL-EX175, 3-LCD projector for the fringe projection. The projector has the brightness of 3600 ANSI lumens, a contrast ratio of 2500:1, and a standard resolution of 1024×768 (XGA). An 8-bit CCD camera (AVT Guppy F-146C) was used for image capture. This camera uses a color CCD sensor (Sony ICX267) that produces color images based on the Bayer color filter array technique. And it runs at up to 17.7 fps at full resolution (1392×1040). However, the overlapping spectra between the neighboring channels causes heavy color coupling, and the discrepant behavior of each channel causes imbalance of the three color channels. The image card used in the experiments is MV-1394A, the transmission of which is 400Mb/s.

4.1. Calibration of gray-scale curve

In the fringe-projected techniques for 3D shape measurement, a linear gray-scale curve, which represents the relationship between the input and output gray-scale value, is desired for higher measurement accuracy. However, the intensity response between commercial projectors and CCDs is nonlinear. And the accuracy is affected by color imbalance caused by the mismatch of color spectrum of the projector and camera. So calibration of the gray-scale curve is necessary. We use the method proposed in Ref. [14] to calibrate the gray-scale curve for the red, green and blue channels in our experiments. After calibrating the gray-scale curve, the linearity of the fringe is much better and the background trends of the red, green and blue fringe patterns are approximately the same.

4.2. Contrast experiment

A plaster model of a human face, as shown in Fig. 5 (b), was used as the tested object. A triple-frequency color fringe pattern with 1:3:9 carrier frequency ratio (the pixel periods of the red, green and blue channel fringes are 81, 27 and 9 pixels, whereas the real periods are 45, 15 and 5 mm, respectively) was projected onto the tested object by a 3-LCD projector. The deformed fringe pattern captured by CCD was analyzed using the proposed method.

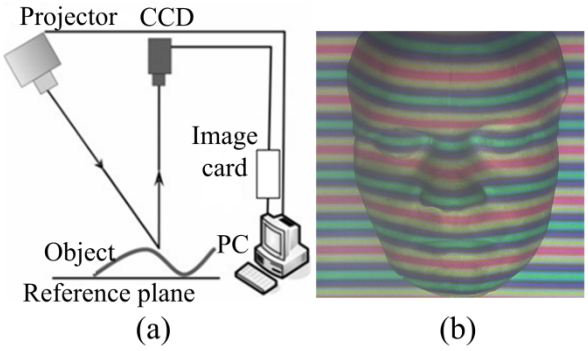

Fig. 5 (a) Experimental setup and (b) deformed color fringe pattern.

Then the image was sent to the computer, and separated into red, green and blue fringe patterns as shown in Fig. 6(a)–6(c). The color decoupling algorithm based on BEMD was used to extract the fundamental frequency components and the accurate results are shown in Fig. 6(d)–6(f). Accordingly, three wrapped phase maps were demodulated via 2D Fourier transform and shown in Fig. 7(a)–7(c). Using the three-step phase unwrapping strategy, the unwrapped phase distribution of the low, medium and high-frequency fringes as shown in Fig. 7(d)–7(f) were acquired.

A four-step-phase-shifting method was used for comparison to prove the feasibility of the proposed technique. The 3D reconstruction of the restored phase distribution obtained by the two methods is shown in Fig. 8. Fig. 8(a) and 8(b) show the restored phase distribution by the four-step-shifting and proposed method, respectively, whereas Fig. 8(c) shows the results of the 256th column. The results reveal that the unwrapped phase is successfully retrieved by the proposed method. However, in the areas close to the borders, the results are not perfect because the results of envelope estimation using RBF interpolation is different from the actual fringe curve in which the height is dramatically changed. Fig. 8(d) shows a detailed view of A with height abrupt, which is one part of 8(c).

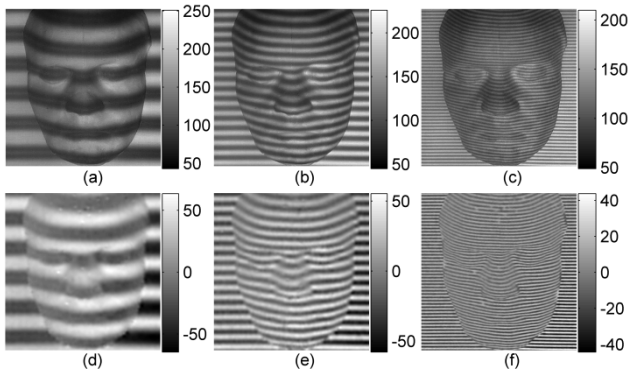

Fig. 6 (a) Red, (b) green and (c) blue fringe patterns from the captured image, and (d) low, (e) medium and (f) high fundamental frequency components extracted by color decoupling algorithm based on BEMD.

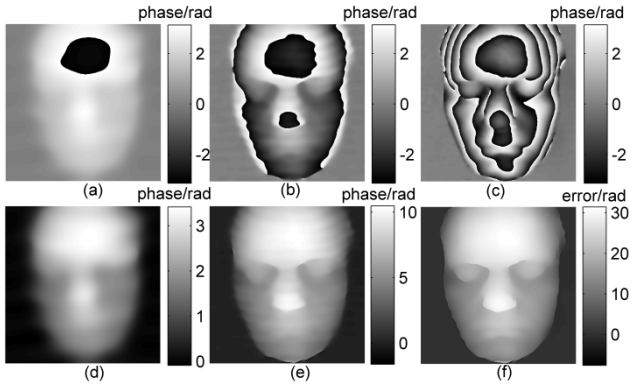

Fig. 7 Wrapped phase maps of (a) low, (b) medium and (c) high-frequency fringes, and unwrapped phase maps of (d) low, (e) medium and (f) high-frequency fringes.

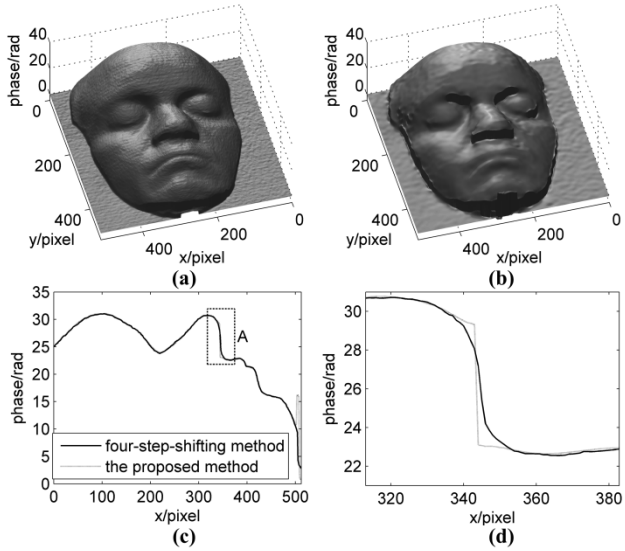

Fig. 8 Restored phase distribution by (a) four-step-shifting method and (b) the proposed method; (c) the results of the 256th column by the two methods and (d) a detailed view of A.

4.3. Experiment on facial expression capture

The technique was also used for facial expression capture. Under the same circumstances as that in the contrast experiment, 66 frames color deformed fringe patterns were continuously captured by CCD camera. Fig. 9(a)–9(c) show only three frames of them (namely surprised, sad and chuckle expressions). The 3D reconstruction results of the restored phase distribution of high-frequency fringes are shown in Fig. 9(d)–9(f). The unwrapped phase is successfully restored, except for some areas close to the borders and other areas with texture abrupt, such as the teeth, eyes and tongue. These results are caused by the inherent defect of fringe-projected techniques, which are not qualified for measuring the objects with texture abrupt.

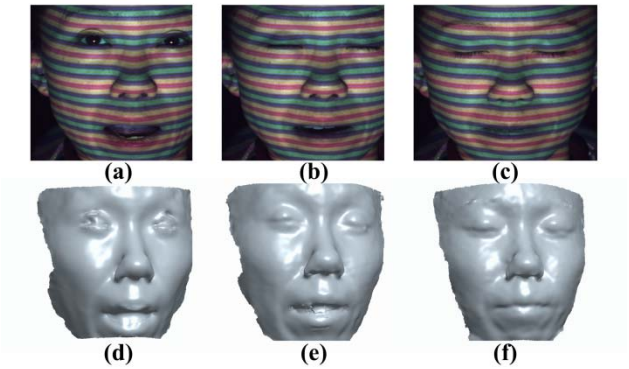

Fig. 9 (a) Surprised, (b) sad and (c) chuckle expressions; 3D reconstruction results of (d) surprised, (e) sad and (f) chuckle expressions.

5. Conclusions

The paper proposed a color fringe-projected technique with the potential for dynamic 3D shape measurement of human faces. The cross talk among color channels of commercial CCD and projector is modeled as the color coupling equations. Then FFT-Spectrum minimization and bi-dimensional empirical mode decomposition (BEMD) are employed to solve the equations. Using three-step phase unwrapping strategy, the unwrapped phase distribution of the high-frequency fringe is recursively acquired to recover the object's height distribution. Only commercial off-the-shelf projector and CCD are needed, so the hardware cost is greatly decreased compared with the previous techniques using light filter and 3-chip CCD. This technique can be implemented for 3D shapes measurement of objects with large discontinuity or spatially isolated surfaces. Apart from the shape, textures of objects are as well retrieved, facilitating 3D real construction combined with textures. The algorithm is accelerated by GPU parallel computation, fulfilling so far 1 frame/s 3D real reconstruction. Since only a single snapshot is required, the technique allows the instantaneous measurement of 3D shapes for fast-moving dynamic objects.

Acknowledgments

This research is supported by the National Natural Science Foundation (Grant No. 51105301) and the National Basic Research Program (Grant No. 2011CB706805) of China. We also acknowledge the support from the Innovation Fund for Undergraduate Research Training and Practice, Xi'an Jiaotong University.

References

1. E. Stoykova, A. A. Alatan, P. Benzie, N. Grammalidis, S. Malassiotis, J. Ostermann, S. Piekh, V. Sainov, C. Theobalt, T. Thevar, and X. Zabulis, "3-D time-varying scene capture technologies - a survey," ed, 2007, pp. 1568-1586.
2. S. Zhang, "Recent progresses on real-time 3D shape measurement using digital fringe projection techniques," *Optics and Lasers in Engineering,* vol. 48, pp. 149-158, 2010.
3. M. Takeda and K. Mutoh, "Fourier transform profilometry for the automatic measurement of 3-D object shapes," *Appl. Opt.,* vol. 22, pp. 3977-3982, 1983.
4. W.-H. Su and H. Liu, "Calibration-based two-frequency projected fringe profilometry: a robust, accurate, and single-shot measurement for objects with large depth discontinuities," *Opt. Express,* vol. 14, pp. 9178-9187, 2006.
5. M. Takeda, Q. Gu, M. Kinoshita, H. Takai, and Y. Takahashi, "Frequency-multiplex Fourier-transform profilometry: a single-shot three-dimensional shape measurement of objects with large height discontinuities and/or surface isolations," *Appl. Opt.,* vol. 36, pp. 5347-5354, 1997.
6. H.-M. Yue, X.-Y. Su, and Y.-Z. Liu, "Fourier transform profilometry based on composite structured light pattern," *Optics & Laser Technology,* vol. 39, pp. 1170-1175, 2007.
7. J. Pan, P. S. Huang, and F.-P. Chiang, "Color phase-shifting technique for three-dimensional shape measurement," *Optical Engineering,* vol. 45, p. 013602, 2006.
8. L. Kinell, "Multichannel method for absolute shape measurement using projected fringes," *Optics and Lasers in Engineering,* vol. 41, pp. 57-71, 2004.
9. P. S. Huang, Q. Hu, F. Jin, and F.-P. Chiang, "Color-encoded digital fringe projection technique for high-speed three-dimensional surface contouring," *Optical Engineering,* vol. 38, pp. 1065-1071, 1999.
10. Z. Zhang, D. P. Towers, and C. E. Towers, "Snapshot color fringe projection for absolute three-dimensional metrology of video sequences," *Appl. Opt.,* vol. 49, pp. 5947-5953, 2010.
11. Z. Zhang, C. E. Towers, and D. P. Towers, "Time efficient color fringe projection system for 3D shape and color using optimum 3-frequency Selection," *Opt. Express,* vol. 14, pp. 6444-6455, 2006.
12. W.-H. Su, "Projected fringe profilometry using the area-encoded algorithm for spatially isolated and dynamic objects," *Opt. Express,* vol. 16, pp. 2590-2596, 2008.
13. W.-H. Su, "Color-encoded fringe projection for 3D shape measurements," *Opt. Express,* vol. 15, pp. 13167-13181, 2007.
14. P. S. Huang, C. Zhang, and F.-P. Chiang, "High-speed 3-D shape measurement based on digital fringe projection," *Optical Engineering,* vol. 42, pp. 163-168, 2003.
15. N. Karpinsky, S. Lei, and S. Zhang, "High-resolution, real-time fringe pattern profilometry," Singapore, Singapore, 2009, pp. 75220E-9.
16. X. Zhou, A. G. Podoleanu, Z. Yang, T. Yang, and H. Zhao, "Morphological operation-based bi-dimensional empirical mode decomposition for automatic background removal of fringe patterns," *Optics Express,* vol. 20, pp. 24247-24262, 2012
17. H. Zhao, W. Chen, and Y. Tan, "Phase-unwrapping algorithm for the measurement of three-dimensional object shapes," *Appl. Opt.,* vol. 33, pp. 4497-4500, 1994.
18. P. S. Huang, Q. Hu, F. Jin, and F. P. Chiang, "Color-encoded digital fringe projection technique for high-speed three-dimensional surface contouring," *Optical Engineering,* vol. 38, p. 1065, 1999.